Electronic Supplementary Material (ESI) for Materials Advances.

Shellac Mediated Laser Induced Reduced Graphene Oxide Film on Paper and Fabric: Exceptional Performance in Flexible Fuel Cell, Supercapacitor and Electrocardiography Applications

Pavar Sai Kumar[1], Vanmathi S[1], Himanshi Awasthi[1], Imran Khan[1], Ritesh Kumar Singh[1], Vimal Kumar Sharma[2], Chandrani Pramanik[2*] and Sanket Goel[1*]

[1]MEMS, Microfluidics and Nanoelectronics (MMNE) Lab, Department of Electrical and Electronics Engineering, Birla Institute of Technology and Science (BITS) Pilani, Hyderabad Campus, Hyderabad 500078, India

[2] Graphene Centre, Tata Steel Limited, Jamshedpur, Jharkhand, 831007, India

1st *Corresponding Author's Email Address: sgoel@hyderabad.bits-pilani.ac.in

2nd *Corresponding Author's Email Address: chandrani.pramanik@tatasteel.com

Supplementary Information

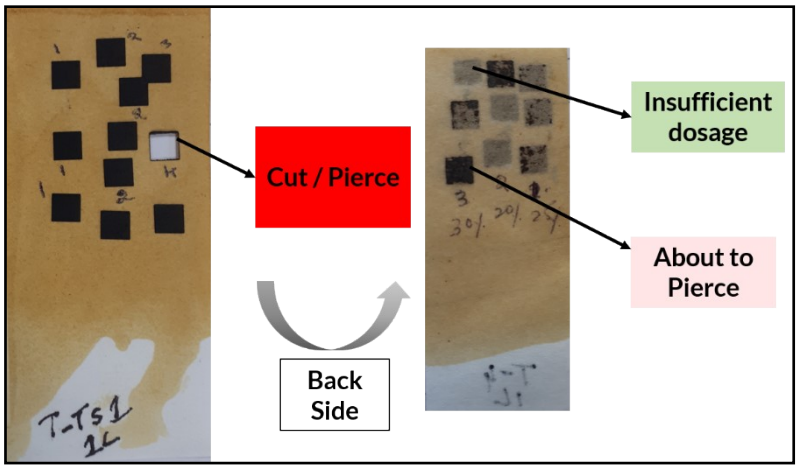

Fig. S1. Optimizations of laser parameters to obtain the high-quality graphenized material. The laser irradiated shellac coated paper substrates indicate the significance of laser parameters ('–' Insufficient dosage; ' × ' Higher dosage (i.e., substrate cut, discarded); representations used in the main text).

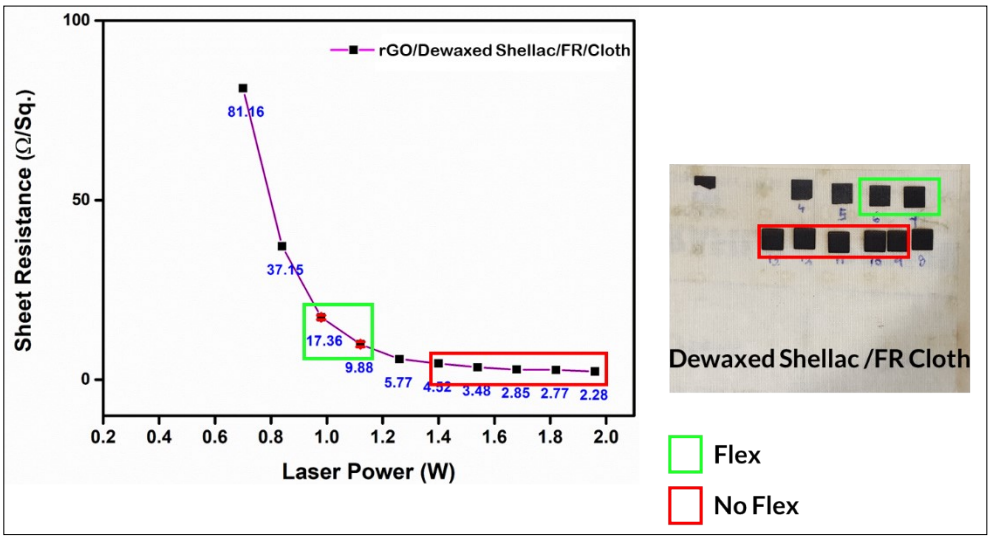

Fig. S2. Effect of laser power on the sheet resistance of rGO/Dewaxed Shellac/FR/Cloth; Flex: regions where the formed rGO was stable on bending; No Flex: regions where the formed rGO was peeling off on bending.

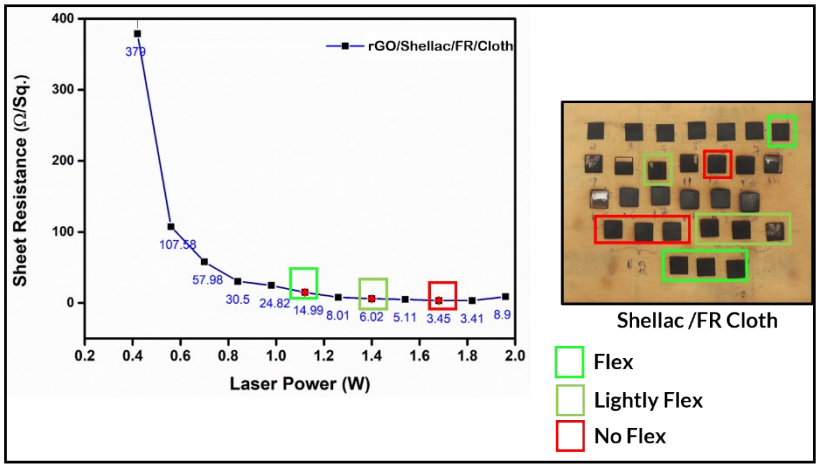

Fig. S3. Effect of laser power on the sheet resistance of rGO/Shellac/FR/Cloth; Flex: regions where the formed rGO was stable on bending; Lightly Flex: regions where the bending was minimum possible; No Flex: regions where the formed rGO was peeling off on bending.

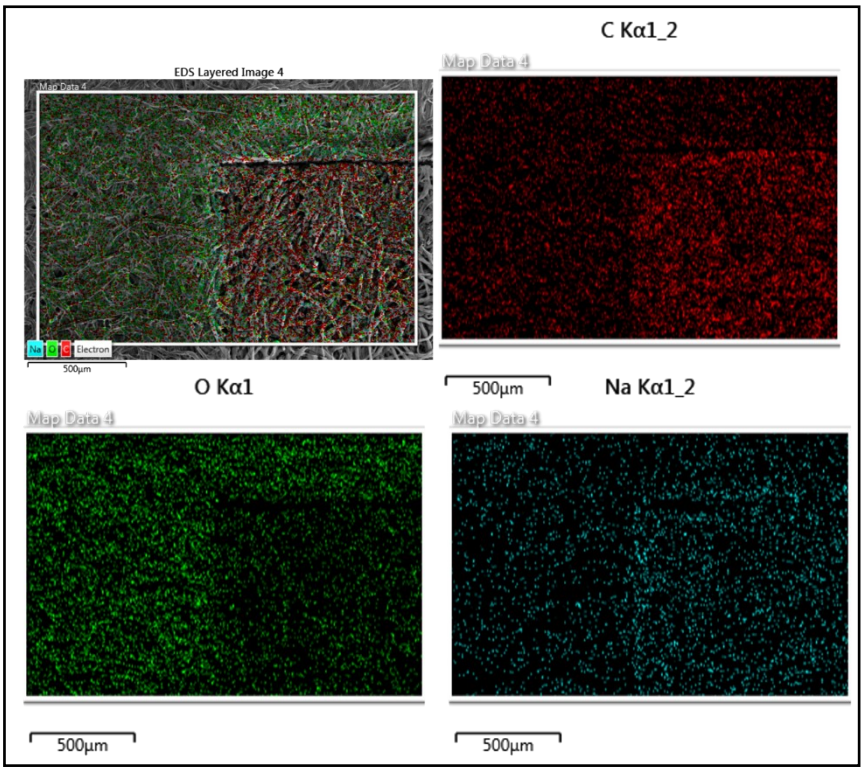

Fig. S4. Elemental composition analysis of rGO/Dewaxed Shellac/FR/Paper; The observations show uniform elemental distributions of all elements combined, and the carbon (c), oxygen (O), and sodium (Na) are shown, respectively.

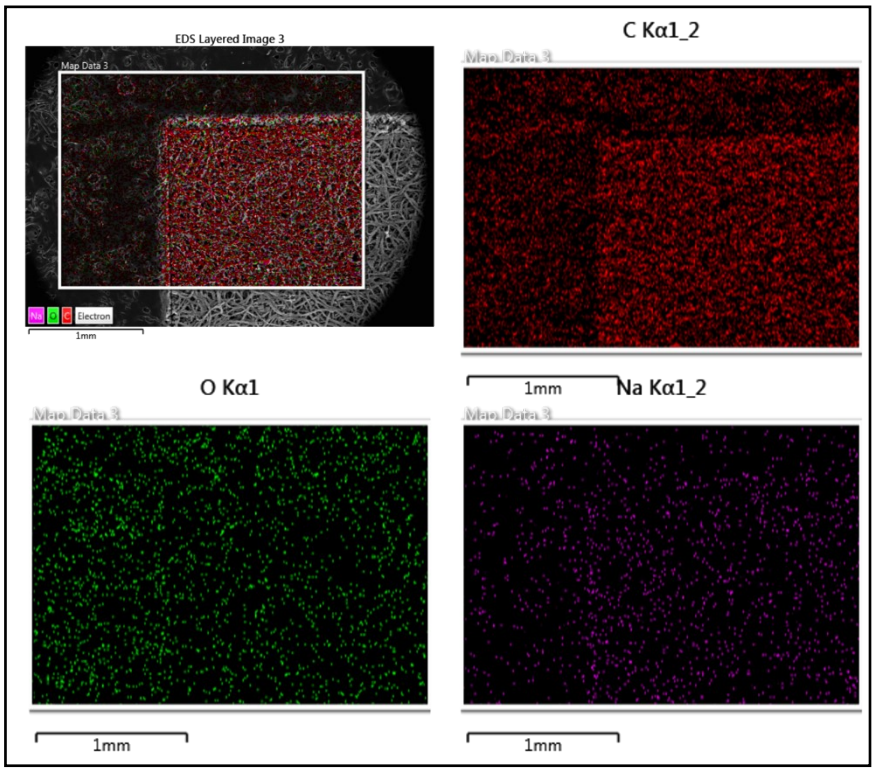

Fig. S5. Elemental composition analysis of rGO/Shellac/FR/Paper; The observations show uniform elemental distributions of all elements combined, and the carbon (c), oxygen (O), and sodium (Na) are shown, respectively.

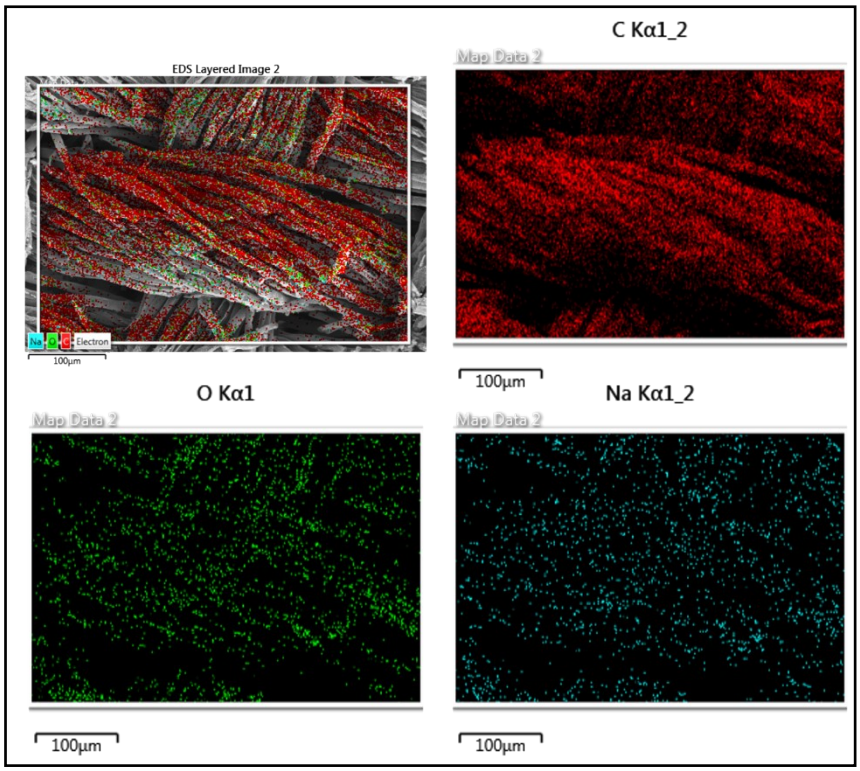

Fig. S6. Elemental composition analysis of rGO/Dewaxed Shellac/FR/Cloth; The observations show uniform elemental distributions of all elements combined, and the carbon (c), oxygen (O), and sodium (Na) are shown, respectively.

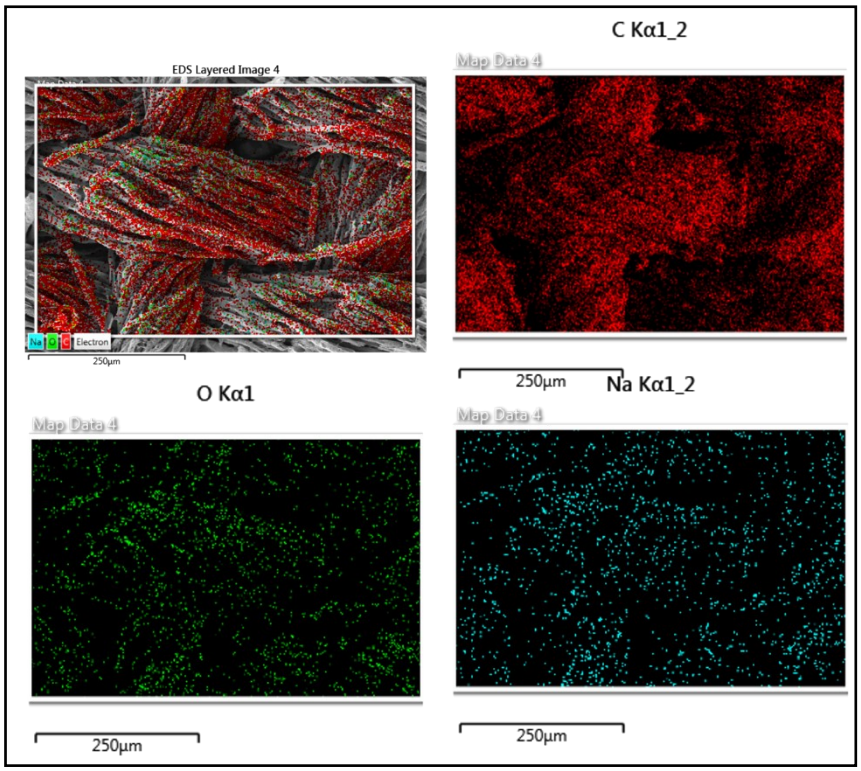

Fig. S7. Elemental composition analysis of rGO/Shellac/FR/Cloth; The observations show uniform elemental distributions of all elements combined, and the carbon (c), oxygen (O), and sodium (Na) are shown, respectively.

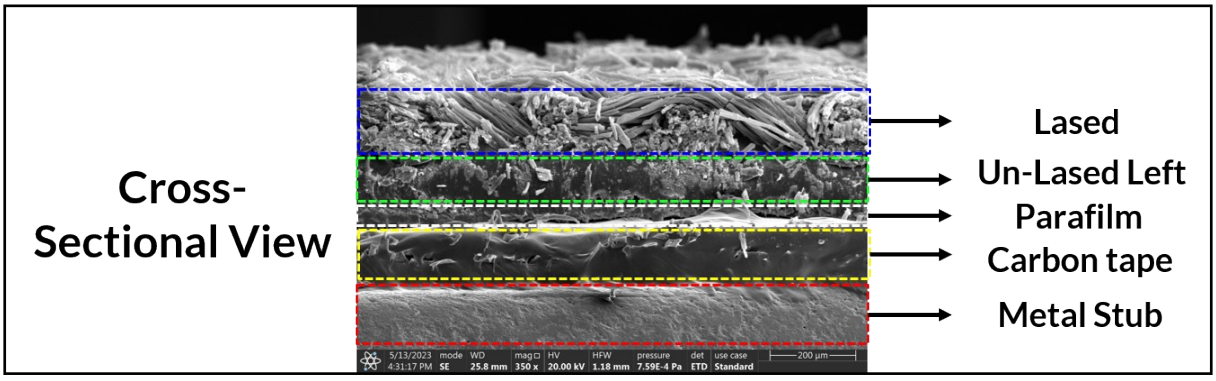

Fig. S8. Cross-sectional representation of the developed laser irradiated rGO on biopolymer treated cloth sample.

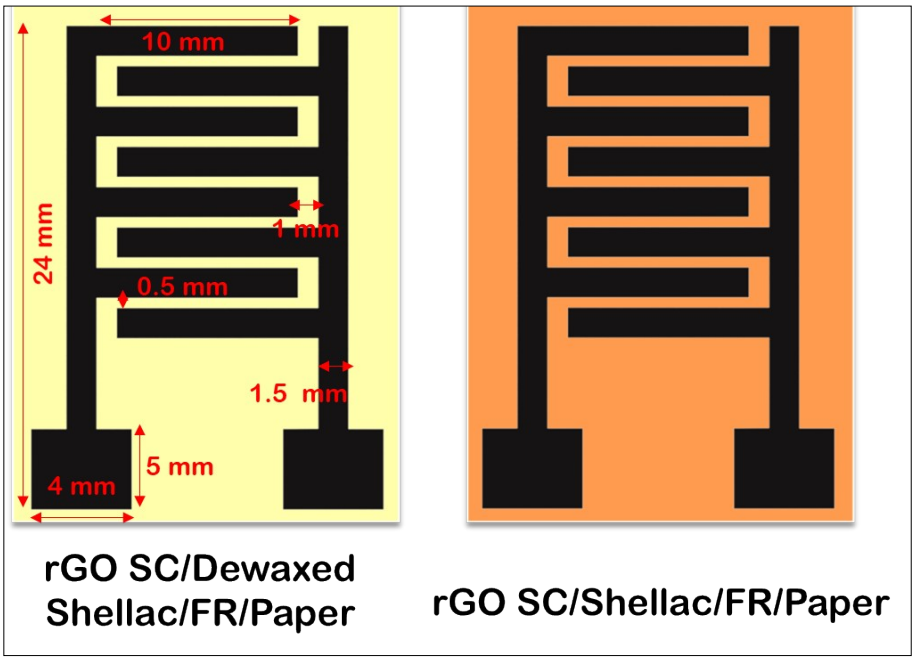

Fig. S10. Supercapacitor device design on Dewaxed Shellac and Shellac paper substrates; rGO = reduced graphene oxide, SC = supercapacitor. (All dimensions are in mm)

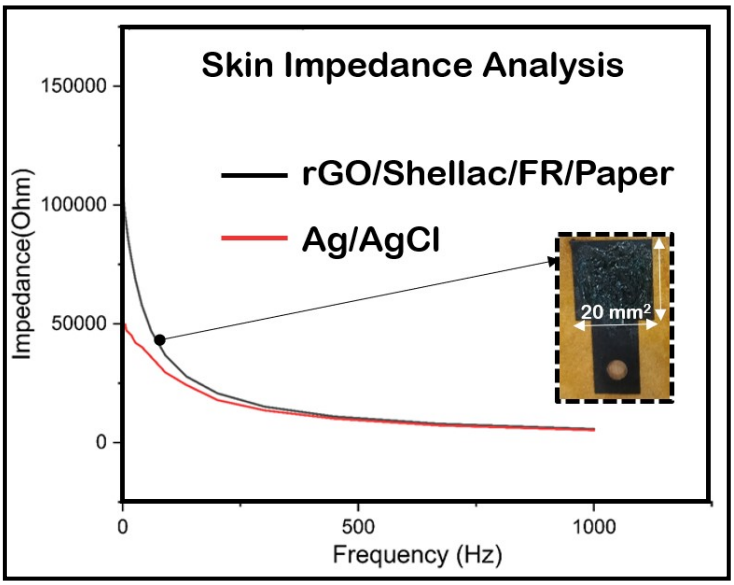

Fig. S11. Skin impedance analysis of the rGO/Shellac/FR/Paper and Ag/AgCl electrodes (Inset: working rGO electrodes).

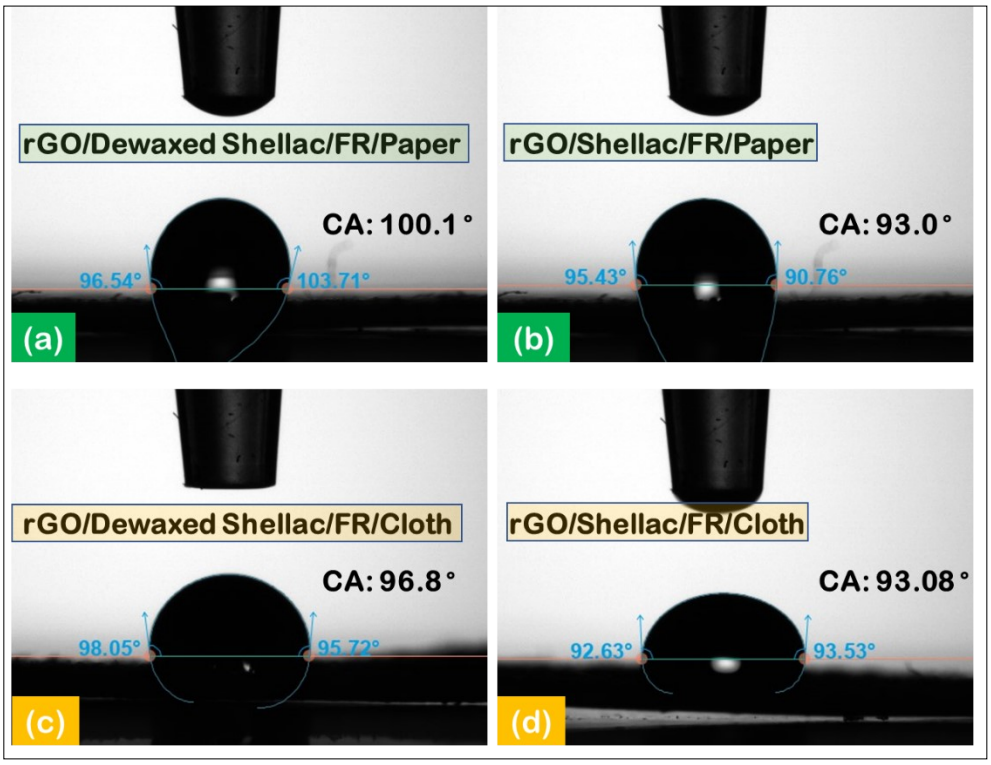

Fig. S12. Wetting angle characteristics, (a) rGO/Dewaxed Shellac/FR/Paper with a mean contact angle (CA) of 100.1 °, (b) rGO/Shellac/FR/Paper showed a mean CA of 93.0 °, (c) rGO/Dewaxed Shellac/FR/Cloth showed a mean CA of 96.8 °, and (d) rGO/Shellac/FR/Cloth showed a mean CA of 93.08 °.

Section 1:

1.1. Temperature Stability Analysis

The temperature stability analysis was carried out on the rGO/Shellac/FR/Paper by developing the resistive model, as shown in Fig. S13. The width of the sensor is 0.5 mm in thickness, and the overall dimensions include 30 mm × 20 mm, shown in inset Fig. S13 a. Further, the experimental conditions include a hotplate for temperature governing, an LCR meter to obtain the variation in resistance due to change in temperature, and the developed sensor enclosed by a glass petri dish, shown in Fig. S13 b. The ambient standard resistance value (Z_0) was obtained at 25 ℃ initially before applying the temperature variations. Further, the resistance (Z) change with the standard was obtained by applying the temperature variations from 30 ℃ to 100 ℃ at a step of 5 ℃. Fig. S13 a show the $\Delta Z/Z_0$ variations with the application of temperatures ($\Delta Z = Z - Z_0$). It was observed that at a fixed frequency of 10 KHz (i.e. in the audible sonic range), the step up or increase in temperatures showed a decrease in the $\Delta Z/Z_0$ values. However, in the

reverse, during the step-down or cooling of the temperatures, it was observed that the mapping of step-up trace was possible with the satisfactory R^2 fit of 0.9433.

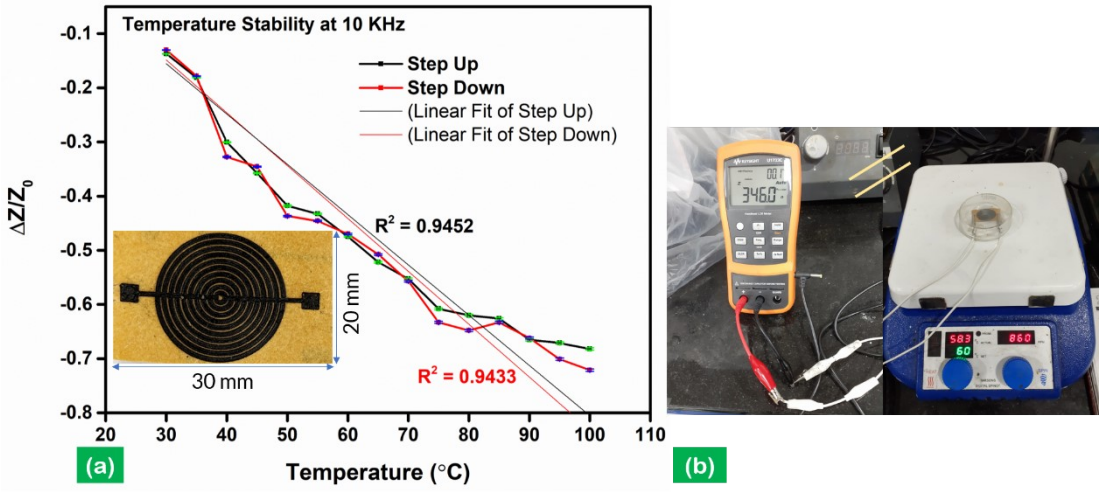

Fig. S13. Temperature stability analysis on a resistive sensor rGO/Shellac/FR/Paper.

1.2. Antibacterial Studies

The antibacterial studies were performed via agar diffusion plate testing methodology on the developed 120 mm × 120 mm sheets of rGO/Shellac/FR/Paper and rGO/Dewaxed Shellac/FR/Paper samples. The experimenting parameters include the test sample size of 25 mm ± 5 mm discs of the samples, test bacterial organisms Staphylococcus aureus ATCC 6538 and Klebsiella pneumoniae ATCC 4352, specimen conditioning for 24 hrs in a sterile petri dish at room temperatures and the incubation conditions of 37 ℃ for 24 hrs. All of the subjected samples showed the inhibition zone exceeding 1 mm or up to 1 mm with the assessment of good effect, summarized in Supplementary Table 1.

Supplementary Table 1: Antibacterial activities of rGO/Shellac and Dewaxed Shellac paper samples

			Zone of inhibition (mm)	Growth under specimen	Antibacterial effect Assessment
rGO/Dewaxed Shellac/FR/Paper	Staphylococcus acureus	Side 1: Coated Side	Absent	Absent	Good Effect
		Side 2: Non-coated	Absent	Absent	Good Effect

		side			
	Klebsiella pneumoniae	Side 1: Coated Side	Absent	Absent	Good Effect
		Side 2: Non-coated side	Absent	Absent	Good Effect
	Staphylococcus acureus	Side 1: Coated Side	Absent	Absent	Good Effect
		Side 2: Non-coated side	Absent	Absent	Good Effect
rGO/Shellac/FR/Paper	Klebsiella pneumoniae	Side 1: Coated Side	Absent	Absent	Good Effect
		Side 2: Non-coated side	Absent	Absent	Good Effect
Inhibition Zone (mm) mean value: (>1), Growth under specimen: None, Description: Inhibition zone exceeding 1mm, no growth, Assessment: Good effect. Inhibition Zone (mm) mean value: (1-0), Growth under specimen: None, Description: Inhibition zone up to 1mm, no growth, Assessment: Good effect.					

Section 2:

2.1. Material Characterizations

The developed biopolymer assisted rGO material was thoroughly characterized to analyze its physical and chemical properties. The crystalline and lattice information was derived from X-ray diffraction (XRD) analysis (Ultima-IV, Rigaku, Australia). The XRD study was performed using a Cu (Cu-Kα, 0.154 nm) target with a scan speed of 2 °/min from 5 ° to 80 ° 2θ positions. X-ray photoelectron spectroscopy (XPS) analysis (K-Alpha, Thermo Fisher Scientific, UK), with an Al-Kα target, was carried out to obtain the elemental composition and interface bonding investigations. The optical transitions were obtained from the absorbance spectra of UV-Vis spectroscopic analysis (V-650, Jasco, USA). The scan speed for the dispersed material phase into ethanol was 200 nm/min, ranging from 200 nm to 800 nm. Brunauer-Emmett-Teller

(BET) analysis was performed to obtain the specific surface area (SSA) through (77.3 K) nitrogen gas adsorbate (N2) sorption isotherms. Barret-Joyner-Halenda (BJH) analysis was carried out on the obtained sorption isotherms to obtain the pore size distribution analysis (BEL SOEP mini II, Microtrac Bel, Japan). The surface morphological images were captured and analyzed using field emission scanning electron microscopy (FESEM) (Apreo LoVac, FEI, USA), and the higher magnification images were obtained from Transmission electron microscopy (Thermo Fisher Scientific, Talos F200X, Japan) operated at 200 KeV. The characteristic peaks for the obtained rGO material were captured using Raman spectroscopy with an excitation wavelength of 633 nm at a magnification of 50X (Witec-alpha-300-ACCRSS, Germany). The surface wetting angle measurements were performed using a benchtop tensiometer (Theta lite, Biolin Scientific, Sweden). All the conductivity and sheet resistance characterizations were carried out via a four-probe conductivity meter with a mean of 25 iterations (T2001A3, Ossila Sheffield, UK).

Section 3:

Supplementary Table 2 and Supplementary Table 3 represent the optimization of laser power at an optimized laser speed of 40 mm/s on biopolymer assisted cloth substrates.

Supplementary Table 2: Optimization of laser parameters on “DS”/FR/Cloth.

LIrGO/ Dewaxed shellac/FR/Cloth		
“DS” : IPA (w/v)		(1:5)
Laser Power (%)	Laser Power (W)	Avg. Sheet Resistance (Ω/Sq.) (n=3)
15	0.42	–
20	0.56	–
25	0.7	81.2
30	0.84	37.6
35	0.98	17.4
40	1.12	9.9

45	1.26	5.8 (~ ×)
50	1.4	4.5 (~ ×)
55	1.54	3.5 (~ ×)
60	1.68	2.9 (~ ×)
65	1.82	2.8 (~ ×)
70	1.96	2.3 (~ ×)

'–' Insufficient dosage; '~ × ' A bit of higher dosage (i.e., observation of minor substrate cut); Laser max. Power: 2.8 W; Laser max. Speed (300 %): 120 mm/s; LIrGO: Laser Induced rGO.

Supplementary Table 3: Optimization of laser parameters on "S"/FR/Cloth.

LIrGO/Shellac/FR/Cloth			
"S" : IPA (w/v)			(1:5)
Laser Power (%)	Laser Power (W)	Laser Speed (%)	Avg. Sheet Resistance (Ω/Sq.) (n=3)
15	0.42	100 % or 40 mm/s	379.3
20	0.56		107.6
25	0.7		57.9
30	0.84		30.5
35	0.98		24.9
40	1.12		14.9
45	1.26		8.1
50	1.4		6.1 (~ ×)
55	1.54		5.2 (~ ×)
60	1.68		3.5 (~ ×)

65	1.82		3.4 (~ ×)
70	1.96		×

'–' Insufficient dosage; '~ ×' A bit of higher dosage (i.e., observation of minor substrate cut); ' × ' Higher dosage (i.e., substrate cut, discarded); Laser max. Power: 2.8 W; Laser max. Speed (300 %): 120 mm/s; LIrGO: Laser Induced rGO.

Section 4:

The average crystallite size calculation of (0 0 2) respective planes was estimated using the standard Debey Scherre mathematical equation,

$$D_{avg.} = \frac{K\lambda}{\beta\, Cos(\theta)}$$

Where k = 0.9 (shape factor), λ = 0.15406 nm, β = full-width half maximum of the respective plane (radians), θ = angle of diffraction. The interplanar spacing calculations for the respective (0 02) planes were obtained using the benchmarked Braggs equation,

$$n\lambda = 2d\, Sin(\theta)$$

Where, n = 1, 2, 3 …, and d = interplanar spacing (nm). Further, the obtained XRD spectra analysis was leveraged in finding the approximate number of rGO layers using the equation,

$$N = \frac{D_{avg.}}{d}$$

Where N = no. of layers, $D_{avg.}$ = average crystallite size or crystal stack height, d = interplanar spacing [1–3]. The broad, intense peak of rGO/Dewaxed shellac/FR/Paper contained the least of ~ 10 layers, and the rGO/shellac/FR/Paper with ~ 17 layers. However, the characteristic intense peaks of rGO/Dewaxed shellac/FR/Cloth contain the highest among all of ~ 77 layers and the rGO/Shellac/FR/Cloth with ~ 68 layers. Supplementary Table 4 depicts the quantitative calculated information altogether.

Supplementary Table 4: XRD calculations of the developed biopolymer assisted LIrGO.

Sample	$k\lambda$ **(nm)**	β **(radians)**	2θ **(degrees)**	θ **(radians)**	$D_{avg.}$ **(nm)**	**d (nm)**	**~N (no. of layers)**

rGO/Dewaxed shellac/FR/Paper	0.14	0.18	27.8	0.242	3.2	0.320	11
rGO/Shellac/FR/Paper	0.14	0.11	27.8	0.242	5.4	0.320	17
rGO/Dewaxed shellac/FR/Cloth	0.14	0.02	27.9	0.243	24.5	0.319	77
rGO/Shellac/FR/Cloth	0.14	0.02	28	0.244	21.4	0.318	68

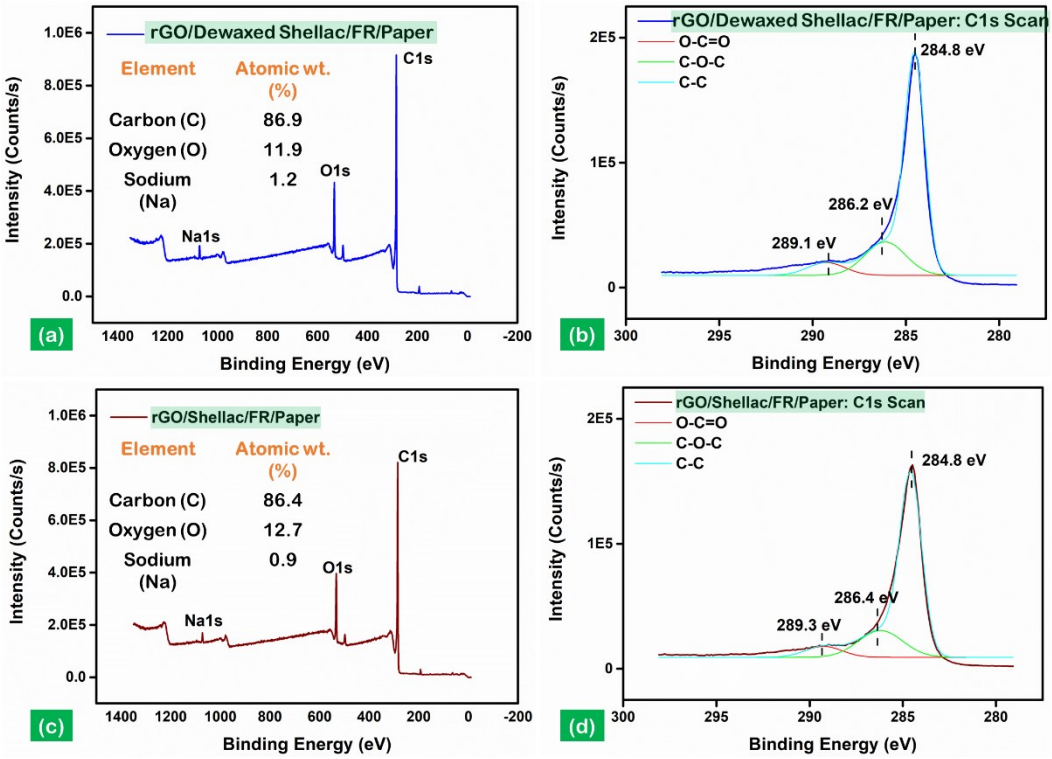

Fig. S14. XPS spectra for the biopolymer assisted LIrGO on paper samples, (a) wide-scan survey of LIrGO/Dewaxed shellac/FR/Paper, (b) deconvoluted narrow scan of C1s spectra of LIrGO/Dewaxed shellac/FR/Paper, (c) wide-scan survey of LIrGO/Shellac/FR/Paper, and (d) deconvoluted narrow scan of C1s spectra of LIrGO/Shellac/FR/Paper.

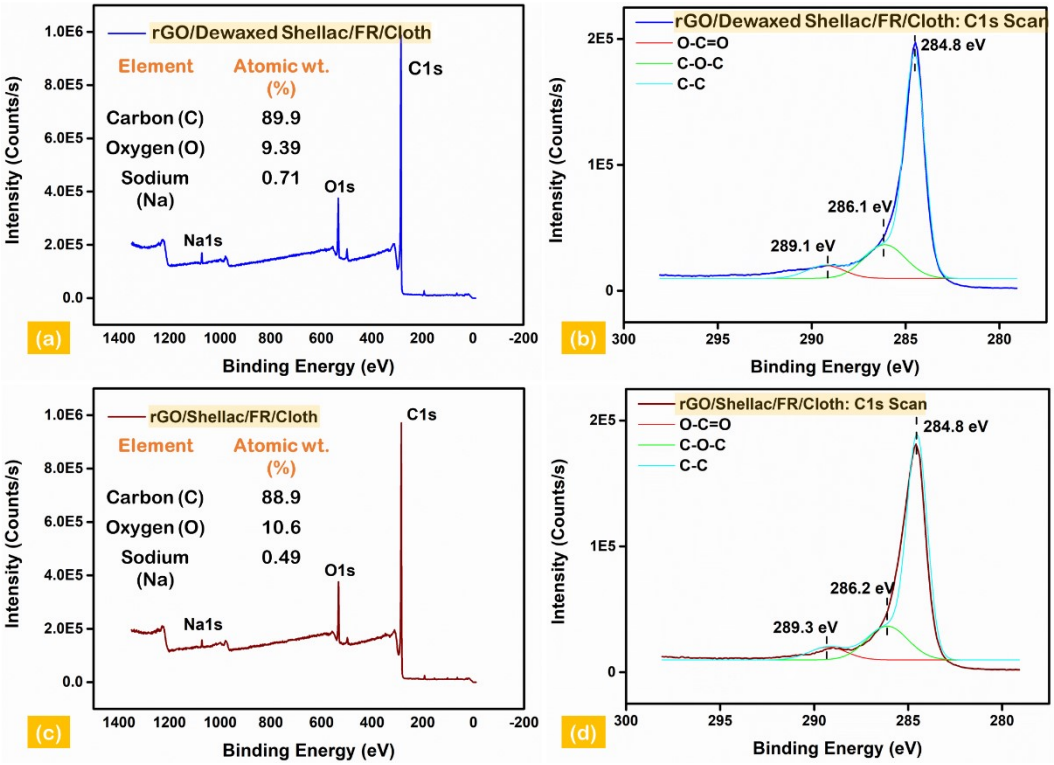

Fig. S15. XPS spectra for the biopolymer assisted LIrGO on cloth samples, (a) wide-scan survey of LIrGO/Dewaxed shellac/FR/Cloth, (b) deconvoluted narrow scan of C1s spectra of LIrGO/Dewaxed shellac/FR/Cloth, (c) wide-scan survey of LIrGO/Shellac/FR/Cloth, and (d) deconvoluted narrow scan of C1s spectra of LIrGO/Shellac/FR/Cloth.

Section 5:

Specific surface area and Pore size analysis

The BET analysis was performed on the obtained N_2 sorption (i.e., adsorption and desorption) isotherms to acquire the specific surface area of the rGO developed on biopolymer assisted paper and cloth samples. The samples were pre-treated at 200 ℃ for 2 hrs. before getting the sorption isotherms. Fig. S16 (a and c) and S17 (a and c) show the Type-III sorption isotherms for the rGO/Dewaxed shellac/FR/Paper, rGO/Shellac/FR/Paper samples, rGO/Dewaxed shellac/FR/Cloth, and rGO/Shellac/FR/Cloth, respectively. Further, the linear fit sorption isotherms were leveraged to calculate the respective samples specific surface areas (m^2/g), shown in Fig. S16 (b and d) and S17 (b and d), respectively. The calculations utilized the standard equations,

$$\mathrm{V_m} = \frac{1}{m+i},\ \mathrm{C} = \frac{1}{V_m \times i},\ \text{and SSA} = \frac{V_m \times N \times \sigma}{Molar\ Volume}.$$

Where, V_m = weight/monolayer capacity (cm^3/g), C = BET constant, σ = surface area of adsorbate N_2 (0.162 nm^2), Molar volume = 22400 cm^3 and SSA = specific surface area (m^2/g).

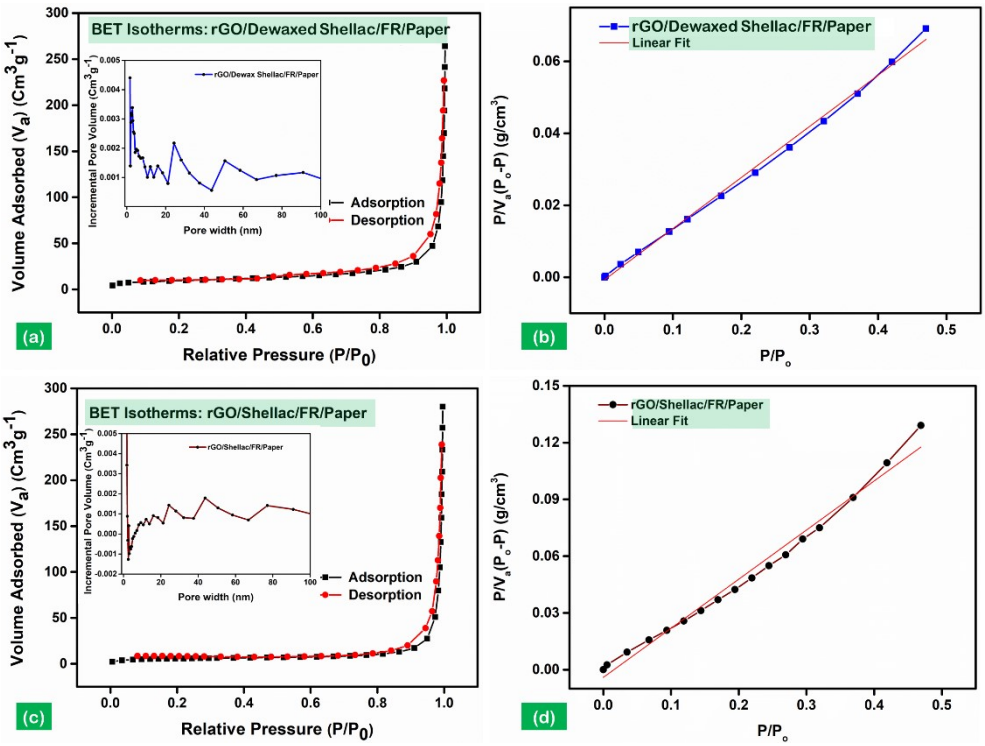

Fig. S16. BET analysis of rGO developed on biopolymer assisted paper samples, (a, b) sorption isotherms of rGO/Dewaxed shellac/FR/Paper (inset: BJH curve of pore size distributions) and a linear fit plot of relative pressures, (c, d) sorption isotherms of rGO/Shellac/FR/Paper (inset: BJH curve of pore size distributions) and a linear fit plot of relative pressures.

Moreover, the rGO/Dewaxed shellac/FR/Paper showed the highest SSA of 33.52 m^2/g while the SSA of 20.83 m^2/g, 28.01 m^2/g, and 32.32 m^2/g corresponds to the rGO/Shellac/FR/Paper, rGO/Dewaxed shellac/FR/Cloth, and rGO/Shellac/FR/Cloth, respectively, shown in Supplementary Table 5. BJH analysis was carried out through the incremental pore volumes to obtain the pore size distributions. In addition, the surface wetting characteristics were analyzed by finding the wetting angles of the respective samples, shown in Supplementary Figure S12. The summary of the samples showed an average pore diameter ranging from mesoporous to macroporous, as shown in Supplementary Table 5.

Supplementary Table 5: Quantitative BET analysis of rGO developed on biopolymer assisted

paper and cloth samples.

Parameters	rGO/Dewaxed shellac/FR/Paper	rGO/Shellac/ FR/Paper	rGO/Dewaxed shellac/FR/Cloth	rGO/Shellac/ FR/Cloth
Adsorbed monolayer volume (Cm^3g^{-1})	7.71	4.79	6.44	7.43
BET Constant (C)	243.16	127.52	82.65	128.84
Specific surface area (a_s) (m^2g^{-1})	33.52	20.83	28.01	32.32
Pore volume (Cm^3g^{-1})	0.40	0.40	0.40	0.48
Average pore diameter (nm)	46.73	71.96	52.65	56.7

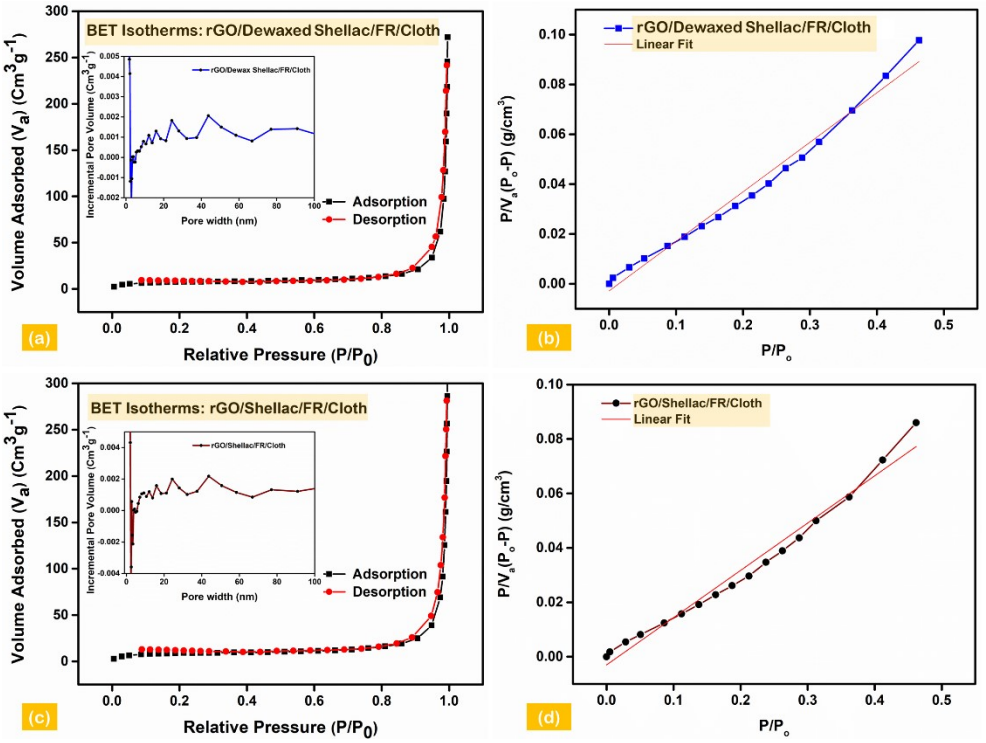

Fig. S17. BET analysis of rGO developed on biopolymer assisted cloth samples, (a, b) sorption isotherms of rGO/Dewaxed shellac/FR/Cloth (inset: BJH curve of pore size distributions) and a linear fit plot of relative pressures, (c, d) sorption isotherms of rGO/Shellac/FR/Cloth (inset: BJH curve of pore size distributions) and a linear fit plot of relative pressures.

Section 6:

Materials and Instrumentation

Mediators, AzBTS-$(NH_4)_2$ (ABTS) and Quinone (PBQ), β-D-Glucose: oxygen 1-oxidoreductase (GO_X) and laccase (LAC) (Aspergillus niger) were procured from Sigma-Aldrich, India. N1 - ((Ethylimino) methylene) - N3 (EDC), 5-pyrrolidine-dione (NHS), Monosodium dihydrogen orthophosphate (NaH_2PO_4), *sec*-Sodium phosphate (Na_2HPO_4), and D-(+)-glucose (99.5%) were purchased from Sisco Research Laboratories (SRL), India. Milli-Q water was used for the preparation of phosphate buffer solution (PBS) 0.1 M, pH (7), throughout the experiments. Plasma system (Femtoscience-CUTE Series, South Korea), Potentiostat (SP-150) biologic potentiostat from Biologic Instruments, France, were used for the study.

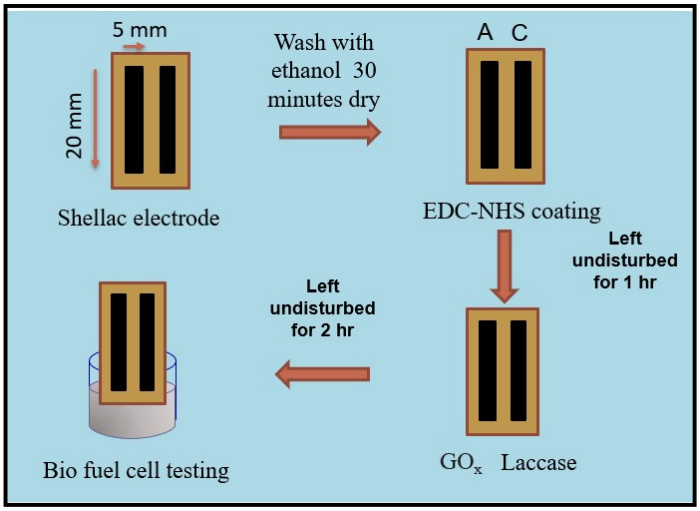

Fig. S9 A. Electrode modification process flow.

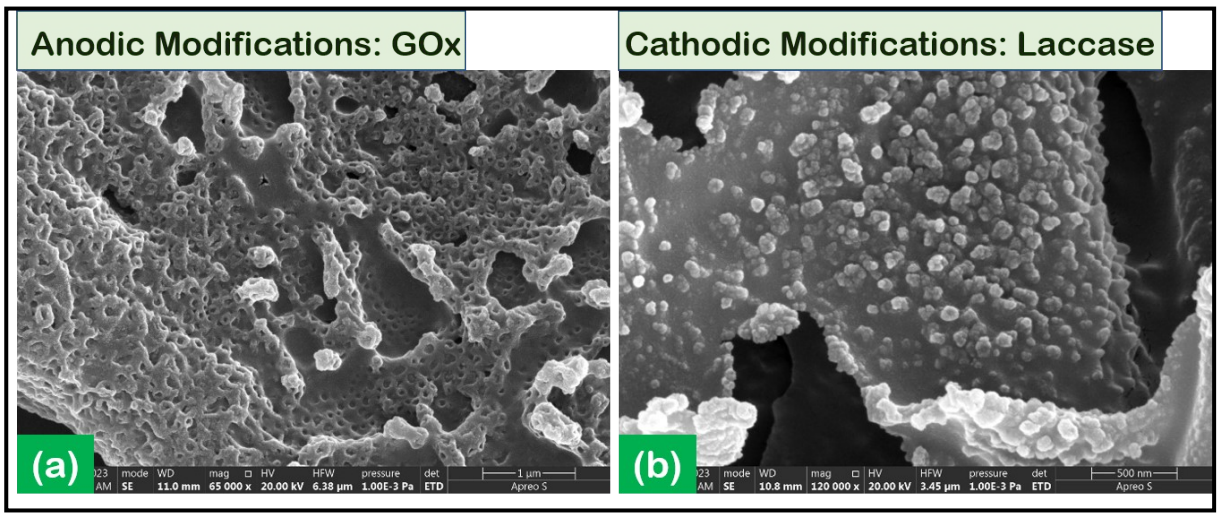

Fig. S9 B. Scanning electron microscopy analysis, (a) anodic GOx modifications and (b) cathodic Laccase modifications.

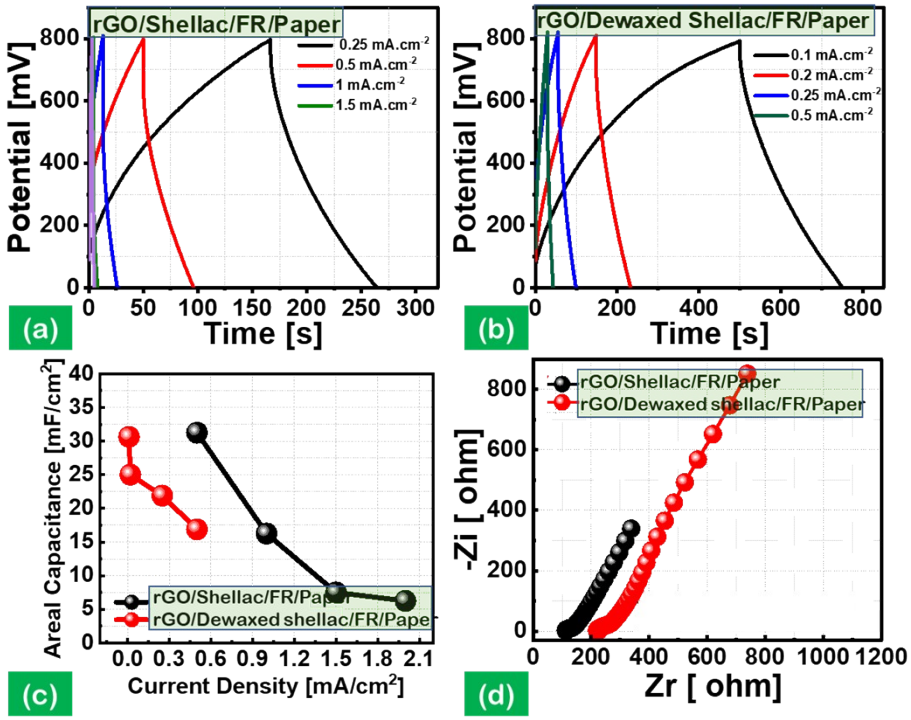

Fig. S18. Galvanostatic characterizations of biopolymer assisted rGO developed on both paper samples, (a) GCD analysis on rGO/Shellac/FR/Paper, (b) GCD analysis on rGO/Dewaxed shellac/FR/Paper, (c) areal capacitance analysis, and (d) electrochemical impedance analysis.

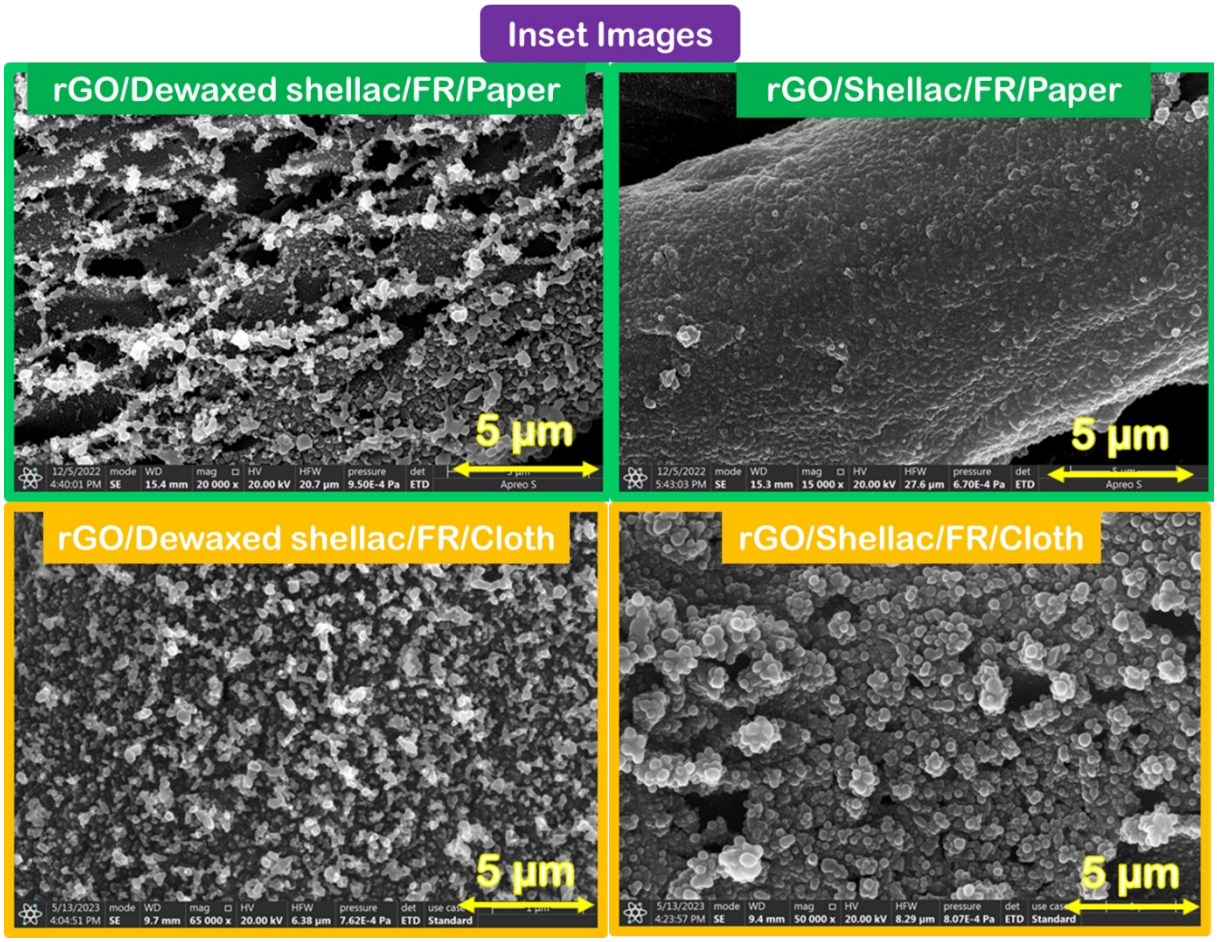

Fig. S19. Inset FESEM images of Main Manuscript Fig. 3, respectively.

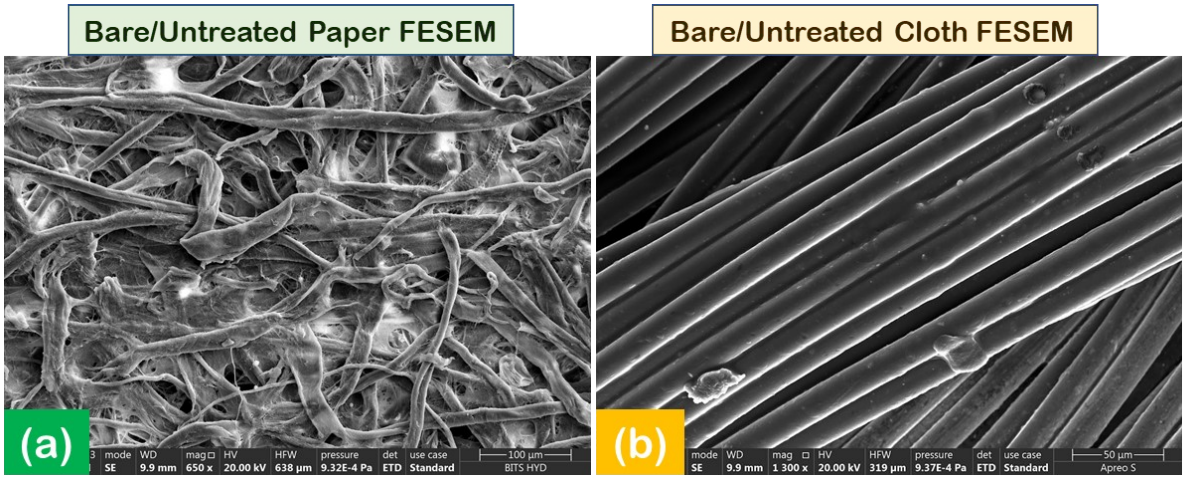

Fig. S20. FESEM images of unmodified samples, a) Untreated (bare) Paper and b) Cloth samples.

References

[1] A. Kaushal, S.K. Dhawan, V. Singh, Determination of crystallite size, number of graphene layers and defect density of graphene oxide (GO) and reduced graphene oxide (RGO), AIP Conf. Proc. 2115 (2019) 30106. https://doi.org/10.1063/1.5112945.

[2] S.Y.T. Trolles-Cavalcante, A. Dutta, Z. Sofer, A. Borenstein, The effectiveness of Soxhlet extraction as a simple method for GO rinsing as a precursor of high-quality graphene, Nanoscale Adv. 3 (2021) 5292–5300. https://doi.org/10.1039/D1NA00382H.

[3] S.H. Huh, X-ray diffraction of multi-layer graphenes: Instant measurement and determination of the number of layers, Carbon N. Y. 78 (2014) 617–621. https://doi.org/https://doi.org/10.1016/j.carbon.2014.07.034.